TITLE Cluster Studies of Chemisorption Using Total Energy Techniques

AUTHOR Adrian Wander

INSTITUTION and DATE University of Warwick 1989

Cluster Studies of Chemisorption Using Total Energy Techniques

Adrian Wander

Submitted for the degree of Doctor of Philosophy

to the University of Warwick

Department of Physics

July 1989

Table of Contents

List of Tables

Figure List

Acknowledgements

I would like to thank Brian Holland, my supervisor, for his excellent guidance and encouragement throughout my time at Warwick. I would also like to thank Vince Dwyer of the University of Loughborough for many helpful discussions during the development of the self consistent ASED scheme, and Phil Smith of the University of Newcastle, Australia for his collaboration in the work on the oxidation of the Si(100) reconstructed surface.

Thanks are also due to all my friends for making my time at Warwick very enjoyable, and for many interesting and exciting discussions. Finally, I would like to thank my parents for their support and encouragement throughout my University career.

Declaration

The work presented in this thesis is my own except where otherwise stated and was performed in the Physics Department, University of Warwick during the period October 1986 to June 1989. No part of this work has previously been submitted to this, or any other, University.

The work on formate and methoxy on Cu(100) presented in Chapter 3 has been published and appeared in Surface Science 199 (1988) L403 and 203 (1988) L637. The work on oxygen on Cu(110) in Chapter 4 has been published in Surface Science 216 (1989) L347 and the work on atomic oxygen on Si(100) presented in Chapter 5 is in press at Surface Science. Finally, the self consistent ASED work presented in Chapter 6 has been submitted to Solid State Communications.

Chapter 1

Introduction

1.1 The Importance of Chemisorption

While bulk solid state properties are relatively well understood, the loss of periodicity created by the formation of an interface can be expected to lead to new and interesting effects. Of these the most dramatic are perhaps the ability of some surfaces to greatly increase the rate of certain chemical reactions (catalysis) and the large scale reconstructions undergone by semiconductor surfaces.

In catalysis, the most important form industrially is heterogeneous catalysis in which the catalyst and the reactants are of different phases. Virtually all such systems studied involve the chemisorption of at least one reactant onto the surface and hence chemisorption is a natural place to start with studies of catalytic systems

[1-3].

One of the main aims of semiconductor device research is the production of smaller and smaller devices. As the linear dimensions of components becomes smaller, surface effects begin to dominate over bulk effects and hence studies of semiconductor surfaces are motivated both by their technological importance and by a desire to obtain a fundamental understanding of reconstruction effects [4].

1.2 Catalysis

The vast majority of catalytically active surfaces are those belonging to the d band metals (noble and transition metals). These materials are readily available and their surfaces are easily cleaned and prepared. Consequently they have been the subject of large numbers of experimental studies.

However, these surfaces are very much harder to handle theoretically. The first complication is the strange intermediate nature of the d shell orbitals. Generally we can divide the electrons around an atom into core and valence (or bonding) parts. The core orbitals are tightly bound to the nucleus and are relatively immune to the presence of neighbouring atoms. They are entirely localised and do not overlap with electron distributions from neighbouring atoms, allowing them to be ignored, or orthogonalised out, in most calculations. (The core-valence separability principle).

The valence electrons are essentially delocalised and overlap strongly with neighbouring atoms. Hence, they can be treated, to a good approximation, as free electrons moving through the solid. This has led to the development of models such as the nearly free electron model and the jellium model.

For d shells the picture becomes more complex. These orbitals have tails which project a long way out of the core region giving rise to large overlaps and hence valence like behaviour. On the other hand they also have maxima in the electron density fairly deep inside the atom which decay rapidly with distance. The properties of this inner region change by relatively small amounts with band formation which is clearly core like behaviour. This mixed behaviour complicates the use of core-valence separability and leads to difficulties in the use of pseudopotential methods which must be adjusted to account for d shell resonances.

These systems also have another drawback. The d shell is often incomplete, and the occupancy can change between the atom and the solid. Also, charge transfer occurs between the substrate and the adsorbate and hence charge self-consistency is of the utmost importance. Consequently theory has, until recently, lagged well behind experimental investigation.

One of the most interesting and important aspects of catalysis is the selectivity displayed by many surfaces. When two or more competing reaction pathways exist, some surfaces will selectively catalyse one while leaving the other unchanged.

Hence, it is possible to selectively produce the desired end product. This selectivity is thought to be due to the formation of stable surface intermediate species such as methoxy (H_3CO) for methanol reactants on copper and formate (HCOO) for formic acid and formaldehyde reactions on copper [5].

The first step in attaining a detailed understanding of these effects at the molecular level is the determination of the surface structure of these intermediates. However, experimental investigations of these structures have led to much controversy over the interpretation of experimental data with several groups proposing different structures for the formate and methoxy radicals on the Cu(100) surface [6-9]. We therefore began by investigating these two systems and propose a bridge site structure for the formate radical [10] and suggest a mixed site occupation for the methoxy group with both the bridge and the hollow site being occupied [11].

Oxygen is obviously of importance both for corrosion studies and as a constituent in many catalytic systems. However,the low temperature structure of oxygen on copper had been the subject of two conflicting experimental studies with both molecular and atomic chemisorption processes having been proposed [12,13]. We therefore then turned to investigate this process and suggest an atomic oxygen structure in which the oxygen atom sits in a long bridge site [14].

1.3 Surface Reconstructions

When a bulk semiconductor is cleaved, the surface undergoes a large scale reconstruction with the surface atoms undergoing large displacements from their bulk terminated positions. (e.g Si(100)(2×1) [15], Si(111)(2×1) [16]).

Oxygen chemisorption on silicon surfaces is of importance to the electronics industry. It obviously forms the basis of much contamination research, but may also be of importance via the electrical properties of the resultant silicon oxide surface layer. Consequently it has been extensively studied both experimentally and theoretically. However, all previous theoretical work has neglected the effects of surface reconstruction and has assumed that the presence of the adsorbate removes the reconstruction effects.

We therefore decided to investigate oxygen chemisorption taking full account of the Si(100)(2×1) reconstruction. This has led to the discovery of a new, low coverage 2×1 structure in which the silicon-silicon surface to sub-surface bonds are tilted by about 12.5° with respect to the surface normal [17].

The wealth of experimental data available on semiconductor surface reconstructions make them ideal candidate structures for testing new methods of calculation. We therefore used the Si(111)(2×1) and GaAs(110)(1×1) surfaces to test our newly formulated self consistent atom superposition and electron delocalisation scheme. These results showed that the presence of charge self consistency did

not lead to a significant improvement in the quality of the results and we therefore propose that the use of Pauling's electronegativity theorem is sufficient for this type of semi-empirical calculation [18].

1.4 Theoretical Methods

Band structure calculations have dominated most of solid state physics. Hence, the natural choice of theoretical approach may appear to be to treat the presence of an adsorbate on a surface as a perturbation to the metal surface band structure. Alternatively, the unit cell could be set up to include the adsorbate and the full band structure calculation could then be performed [19]. Unfortunately this approach is unsuitable for a number of reasons. The main difficulty is the artificial periodicity introduced into the calculations by the use of periodic boundary conditions. Hence, in order to remove unwanted adsorbate-adsorbate interactions it becomes necessary to consider very large unit cells. This situation becomes even worse if defects are to be investigated. However, at this point chemical intuition comes to the rescue.

Obviously, a chemical bond is one atom-atom separation in length and hence, if we are only interested in the nature of the surface chemical bond an alternative suggests itself. Instead of a full band structure calculation, we can model the immediate environment of the adsorbate by a cluster of atoms that represents the

metal surface with appropriate boundary conditions and then apply the techniques of quantum chemistry to the resultant 'super molecule'.

Obviously, the question of choice of boundary conditions is crucial to the rigorous application of cluster techniques and we therefore now turn to a discussion of the available options.

1.5 Clusters and Boundary Conditions

Obviously, the choice of boundary conditions is of fundamental importance to the quality of the results obtained using cluster models in chemisorption studies. Unfortunately, the problem is far from resolved.

In the case of semiconductors, a reasonable estimate can be made by saturating the dangling sp hybrid orbitals with hydrogen atoms which maintain the correct hybridisation of these orbitals [20]. However, even here problems arise due to the electronegativity differences between the surface atoms and the hydrogens leading to a charge transfer which would not be present on the true surface.

For d band metals the situation is even worse, and no rigorous method of treatment exists. Instead, free space boundary conditions are used and the calculations are repeated with increasingly large clusters until the quantities of interest converge. (Due to the charge transfer problems associated with the use of hydrogens in semiconductor research the same procedure should also be adopted).

Fortunately, structural parameters usually converge rapidly, and small clusters are usually sufficient to extract meaningful results.

However, a seemingly ideal alternative exists to clusters and band structures-embedded cluster techniques [21]. These methods treat the neighbourhood of the adsorbate as a cluster and then embed the resultant super molecule into an infinite periodic background. The more sophisticated methods rely on matching the Green's functions for the cluster and adsorbate across the interface. Early methods relied on transforming the molecular orbitals of the cluster into a localised set of bonding orbitals [22]-a process that works for ionic or covalent systems but is impossible for most metals. Subsequent work has shown that this is not neccessary, but as yet, little work has been done with transition metal clusters.

1.6 Overview

It is appropriate at this stage to review the rest of this thesis.

Chapter 2 contains a discussion of ab initio quantum chemistry techniques and in particular the self consistent Hartree-Fock equations. Section 2.2 discusses the Hartree-Fock equations and their matrix form the Roothaan-Hall equations. Section 2.3 deals with the important question of the choice of a basis set for molecular calculations and in section 2.4 we move on to present a brief review of the GAMESS SCF MO package. Finally, section 2.5 deals with methods of moving

beyond HF theory by including electron-electron correlation effects.

Chapters 3, 4 and 5 deal with applications of the ab initio method to real systems. Chapter 3 details calculations performed on the formate and methoxy radicals on the Cu(100) surface, while chapter 4 looks at the controversial topic of the low temperature structure of oxygen on Cu(110). Finally, chapter 5 considers the effects of atomic oxygen chemisorption on the Si(100)(2×1) reconstructed surface.

While the preceding three chapters highlight the virtues of ab initio methods, chapter 6 points out some of their vices and in particular the severe demands they make on computational resources. Alternative semi-empirical techniques are then introduced in the form of the extended Huckel and ASED methods. In particular, we discuss the role of charge self consistency in semi-empirical techniques and show that in contrast to other methods, it has little effect on the quality of results produced using the ASED method.

Finally, we conclude in chapter 7 by reviewing the thesis and suggesting possible future developments to this work, both in terms of interesting systems to investigate and new directions in which the theory could be developed.

Chapter 2

Ab Initio Molecular Orbital Theory

2.1 Introduction

Two ab initio methods of calculation have been used to extract meaningful results from cluster calculations; Hartree-Fock (HF) theory and the Kohn-Sham density functional (KSDF) method usually within the local density (LD) approximation for the exchange correlation potential. The KSDF method provides a method of calculating the ground state electron density (and from it the energy) which is in principle exact [23]. However, the relationship between the density and the energy is not known and it is therefore normal to approximate the exchange-

correlation term as being that due to a local function of the density-usually that of a homogeneous electron gas. This method has been widely used in band structure calculations and is beginning to find more applications in molecular calculations despite some dramatic early failures (i.e. linear water [24] and no binding for C_2 [25]).

On the other hand, HF theory is a single determinant method that can be improved via configuration interaction (CI) to give, again in principle, exact results. Both methods are based around an exact solution of the Hartree problem with the HF theory treating exchange effects in an exact non-local manner but ignoring half the correlation effects, while the KSDF method treats both exchange and correlation effects in an averaged local way.

For my work it was decided that HF theory was a better option for two main reasons. Firstly, it forms the mainstay of modern quantum chemistry and hence it has been widely used and tested and its strengths and limitations are well known. Secondly, being so widely used, a number of large commercial packages are available which implement the technique. We therefore now turn to a discussion of the HF method and its matrix implementation, the Roothaan-Hall equations.

2.2 HF Theory and the Roothaan-Hall Equations

The Hamiltonian for a system of N electrons and M nuclei at position vector (r_i) and (R_A) respectively is given by

$$\hat{H} = -\sum_{i}^{N}\frac{1}{2}\nabla_i^2 - \sum_{A}^{M}\frac{1}{2M_A}\nabla_A^2 - \sum_{i}^{N}\sum_{A}^{M}\frac{Z_A}{r_{iA}} + \sum_{i}^{N}\sum_{j>i}^{N}\frac{1}{r_{ij}} + \sum_{A}^{M}\sum_{B>A}^{M}\frac{Z_A Z_B}{R_{ab}} \quad (2.1)$$

where (M_A) are the masses of the nuclei.

Applying the Born-Oppenheimer approximation allows us to factorise this into nuclear and electronic parts where the electronic Hamiltonian is given by

$$\hat{H}_{elec} = -\sum_{i}^{N}\frac{1}{2}\nabla_i^2 - \sum_{i}^{N}\sum_{A}^{M}\frac{Z_A}{r_{iA}} + \sum_{i}^{N}\sum_{i>j}^{N}\frac{1}{r_{ij}} \quad (2.2)$$

We know that the wavefunction for a system of Fermions should be antisymmetric, and we therefore construct a wavefunction to be a Slater determinant $|\Psi_0>$ made up from a set of spin orbitals (χ_a). We now have a Hamiltonian and a trial wavefunction and hence we can apply the variational principle. Therefore, we need to find the (χ_a)'s that minimise

$$E_0 = <\Psi_0 \mid \hat{H} \mid \Psi_0> = \sum_{a} < a \mid h \mid a > + \frac{1}{2}\sum_{ab} < ab \parallel ab > \quad (2.3)$$

where

$$h = \sum_{i} -\frac{1}{2}\nabla_i^2 - \sum_{i}\sum_{A}\frac{Z_A}{r_{iA}} \quad (2.4)$$

and

$$< ab \parallel ab >= \int d\bar{x}_1 d\bar{x}_2 \chi_a^*(\bar{x}_1)\chi_b^*(\bar{x}_2) r_{12}^{-1}(1 - P_{12})\chi_a(\bar{x}_1)\chi_b(\bar{x}_2) \qquad (2.5)$$

and P_{12} is the operator that interchanges electrons one and two when operating to the right.

This minimisation is subject to the constraint that the spin orbitals remain orthonormal. i.e.

$$< \chi_a \mid \chi_b >= \delta_{ab} \qquad (2.6)$$

This process leads to the Hartree-Fock integro-differential equations

$$h(1)\chi_a(1) + \sum_{b \neq a} [\int d\bar{x}_2 \mid \chi_b(2) \mid^2 r_{12}^{-1}]\chi_a(1) - \sum_{b \neq a} [\int d\bar{x}_2 \chi_b^*(2)\chi_a(2) r_{12}^{-1}]\chi_b(1) = \varepsilon_a \chi_a(1) \qquad (2.7)$$

where $h(1)$ is the kinetic and potential energy of a single electron chosen to be electron one moving in the field of the nuclei. The energy of the orbital χ_a is ε_a.

The first of the two electron terms in (2.7) merely represents the coulomb potential felt by electron one due to the other electrons and is normally written in terms of the coulomb operator

$$J_b(1) = \int d\bar{x}_2 \mid \chi_b(2) \mid^2 r_{12}^{-1} \qquad (2.8)$$

The second term is more complex and arises due to the antisymmetric nature of the wave function. This is the exchange term and may similarly be written in

terms of the exchange operator given by

$$K_b(1)\chi_a(1) = [\int d\underline{x}_2 \chi_b^*(2) r_{12}^{-1} \chi_a(2)]\chi_b(1) \tag{2.9}$$

This allows us to rewrite (2.7) as

$$[h(1) + \sum_{b \neq a} J_b(1) - \sum_{b \neq a} K_b(1)]\chi_a(1) = \varepsilon_a \chi_a(1) \tag{2.10}$$

However, since

$$[J_a(1) - K_a(1)]\chi_a(1) = 0 \tag{2.11}$$

we may remove the restricted summation in (2.10) and rewrite it as

$$f(1)\chi_a(1) = \varepsilon_a(1)\chi_a(1) \tag{2.12}$$

where

$$f(1) = h(1) + \sum_b [J_b(1) - K_b(1)] \tag{2.13}$$

is the Fock operator.

The exact solutions to this equation are the true Hartree-Fock spin orbitals. However, in practice it is only possible to solve (2.12) exactly for atoms, and another approximation is necessary for more complex systems. The spin orbitals are expressed in terms of a (finite) basis set, and only as the size of this set nears completion do we tend towards the best solutions-the Hartree-Fock limit.

For reasons of simplicity we will now only consider the restricted Hartree-Fock formalism, although the theory generalizes in a straightforward manner to unrestricted orbitals.

A restricted set of spin orbitals has the form

$$\chi_s(\underline{x}) = \begin{cases} \psi_j(r)\alpha(\omega) \\ \psi_j(r)\beta(\omega) \end{cases} \tag{2.14}$$

where $\alpha(\omega)$ and $\beta(\omega)$ are spin functions. (i.e. we doubly occupy each of the spatial orbitals with electrons of opposite spin). Fortunately most ground states of molecules have an even number of electrons. For an odd number of electrons we must turn to either unrestricted Hartree-Fock theory in which the constraint of double occupancy is relaxed completely, or to restricted open Hartree-Fock theory in which all but the outermost orbital is doubly occupied, the extra electron being placed in the outer orbital.

To proceed, we first integrate over the spin variables in (2.10) leading to

$$f(1)\psi_j(1) = \epsilon_j\psi_j(1) \tag{2.15}$$

where

$$f(1) = h(1) + \sum_{a}^{N/2}[2J_a(1) - K_a(1)] \tag{2.16}$$

-the spatial integro-differential Hartree-Fock equations.

As shown by Roothaan [26], the introduction of a known basis set leads to a set of matrix equations which can be solved using standard techniques.

Let (ϕ_μ) be a set of k known functions. We may express the unknown ψ's as

a linear combination of these basis orbitals

$$\psi_i = \sum_\mu C_{\mu i}\phi_\mu \tag{2.17}$$

substituting into (2.15), multiplying by $\phi_\nu^*(1)$ and integrating, we obtain the equation

$$\sum_\mu C_{\mu i}\int d\tau_1 \phi_\nu^*(1) f(1)\phi_\nu(1) = \varepsilon_i \sum_\nu C_{\nu i}\int d\tau_1 \phi_\mu^*(1)\phi_\nu(1) \tag{2.18}$$

or in matrix form

$$\mathbf{FC} = \mathbf{SC}\varepsilon \tag{2.19}$$

where $\mathbf{F}$ is the Fock matrix with elements given by [B

$$F_{\mu\nu} = \int d\tau_1 \phi_\nu^*(1) f(1)\phi_\mu(1) \tag{2.20}$$

which is a K×K Hermitian matrix (usually real and symmetric). $\mathbf{S}$ is the overlap matrix given by

$$S_{\mu\nu} = \int d\tau_1 \phi_\nu^*(1)\phi_\mu(1) \tag{2.21}$$

which is also a K×K Hermitian matrix (again usually real and symmetric) and $\mathbf{C}$ is the K×K square matrix of the expansion coefficients $C_{\mu i}$.

Before we can proceed we need an expression for the Fock matrix which is normally written in terms of the charge density matrix $\mathbf{P}$. Consider a closed shell molecule in which each of the orbitals $\psi_a(\mathbf{r})$ is doubly occupied. The charge density is given by

$$\rho(\mathbf{r}) = 2\sum_a^{N/2} |\ \psi_a(\mathbf{r})\ |^2 \tag{2.22}$$

Integrating over all space, we generate the total number of electrons

$$\int d\mathbf{r}\rho(\mathbf{r}) = 2\sum_{a}^{N/2}\int d\mathbf{r} \mid \psi_a(\mathbf{r}) \mid^2 = 2\sum_{a}^{N/2} 1 = N \tag{2.23}$$

Now, substituting (2.17) into (2.22) gives

$$\begin{aligned}
\rho(\mathbf{r}) &= 2\sum_{a}^{N/2}\psi_a^*(\mathbf{r})\psi_a(\mathbf{r}) \\
&= 2\sum_{a}^{N/2}\sum_{\mu}C_{\mu a}^*\phi_\mu^*(\mathbf{r})\sum_{\mu}C_{\mu a}\phi_\mu(\mathbf{r}) \\
&= \sum_{\mu\nu}[2\sum_{a}^{N/2}C_{\mu a}C_{\nu a}^*]\phi_\mu(\mathbf{r})\phi_\nu^*(\mathbf{r}) \\
&= \sum_{\nu\mu}P_{\mu\nu}\phi_\mu(\mathbf{r})\phi_\nu^*(\mathbf{r})
\end{aligned} \tag{2.24}$$

where $P_{\mu\nu}$ is defined as the charge density matrix

$$P_{\mu\nu} = 2\sum_{a}^{N/2}C_{\mu a}C_{\nu a}^* \tag{2.25}$$

Returning to (2.20), we can express the Fock matrix elements as

$$\begin{aligned}
F_{\mu\nu} &= \int d\mathbf{r}_1\phi_\mu^*(1)h(1)\phi_\nu(1) + \sum_{a}^{N/2}\int d\mathbf{r}_1\phi_\mu^*(1)[2J_a(1) - K_a(1)]\phi_\nu(1) \\
&= H_{\mu\nu}^{core} + \sum_{a}^{N/2}2(\mu\nu \mid aa) - (\mu a \mid a\nu)
\end{aligned} \tag{2.26}$$

where

$$H_{\mu\nu}^{core} = \int d\mathbf{r}_1\phi_\mu^*(1)h(1)\phi_\nu(1) \tag{2.27}$$

This core matrix only needs to be calculated once during the iterative cycle since it remains invariant throughout. Inserting the linear expansion (2.17) into the two electron term, we arrive at

$$\begin{aligned} F_{\mu\nu} &= H_{\mu\nu}^{core} + \sum_{\lambda\sigma} P_{\lambda\sigma}[(\lambda\sigma \mid \sigma\lambda) - \frac{1}{2}(\mu\lambda \mid \sigma\nu)] \\ &= H_{\mu\nu}^{core} + G_{\mu\nu} \end{aligned} \tag{2.28}$$

where $G_{\mu\nu}$ contains the two electron contributions to the Fock matrix. i.e. we have an expression for the Fock matrix involving the charge density matrix **P** and two electron integrals of the form

$$(\mu\nu \mid \sigma\lambda) = \int d\tau_1 d\tau_2 \phi_\mu^*(1)\phi_\nu(1) r_{12}^{-1} \phi_\lambda^*(2)\phi_\sigma(2) \tag{2.29}$$

The generation and storage of these quantities constitutes the main computational effort and limitation in the implementation of this method.

We now have the generalized eigenvalue problem

$$\mathbf{FC = SCE} \tag{2.30}$$

to solve which can be achieved using standard techniques. However, the equation is highly non-linear ($\mathbf{F = F(C)}$) and hence an iterative procedure (section 2.4) is necessary.

Finally, it should be mentioned that the restricted Hartree-Fock method is readily extended to open shell systems where the constraint of double occupation

of each spatial orbital is removed. This leads to the Pople-Nesbet equations [27] which are the matrix form of the unrestricted Hartree-Fock (UHF) spatial integro-differential equations.

2.3 Basis Sets

The matrix form of the Hartree-Fock equations has been generated by expressing the unknown spin orbitals in terms of a known set of basis functions about which little has been said. We therefore now turn to a consideration of the available options in the choice of these basis functions.

If the basis set (ϕ_μ) used in (2.17) is complete, then no approximation has been introduced. However, due to the limitations of computer storage and processor time it is necessary to restrict the calculations to an incomplete set. Obviously this means that the calculation is only exact in the subspace spanned by this set, and the 'art' consists of choosing the subspace which will lead to sufficiently accurate results in manageable processor times. The usual option is to choose a set of atomic orbitals based on each of the molecule's constituent nuclei. The problem is, what form should these atomic orbitals take?

In the early days, the natural choice was the use of slater functions (SF) which

are exact solutions to the hydrogen atom problem.

$$\phi^{SF} \sim e^{-\zeta r} \tag{2.31}$$

However, these functions suffer from a serious drawback. The evaluation of two electron, four centre integrals in (2.29) is impossible to perform in an analytic manner and we must resort to numerical integration techniques. This leads to a loss of accuracy and also an increase in computational times and costs.

However, alternatives exist. The use of gaussian functions (GF)

$$\phi^{GF} \sim e^{-\alpha r^2} \tag{2.32}$$

allows us to perform these integrals in a closed analytical manner [28,29], since the product of two gaussians with different centres is merely another gaussian centred somewhere along the line joining the two centres; hence, we can reduce the troublesome four centre integrals to two centre integrals which are much easier to handle.

Unfortunately, gaussians do not have the correct behaviour to model real atomic functions. The slater and gaussian type orbitals differ both in their behaviour at small r and at large r. At $r = 0$, the slater orbital has a finite gradient while the gaussian's gradient goes to zero. At large r, the gaussian decays much faster than the slater function. In particular, it can be shown that at large dis-

tances molecular orbitals should decay as

$$\psi \sim e^{-\beta r} \tag{2.33}$$

the exact form of the slater orbital! Hence, we have a choice between a set of orbitals which are easy to handle computationally but have the wrong behaviour, and a set of functions which have the correct behaviour but are very difficult to handle. The solution of this dilemma is the use of contracted gaussian functions (CGF) which have the correct behaviour in the valence region

$$\phi_\mu^{CGF}(\mathbf{r}) = \sum_{a=1}^{L} d_{\mu a}\phi_a^{GF}(\mathbf{r}) \tag{2.34}$$

where L is the contraction length. In practice, the contraction coefficients ($d_{\mu a}$) are held fixed throughout the course of a calculation allowing us to accurately model the behaviour of the chosen atomic orbital while being able to evaluate the two electron integrals as sums of rapidly evaluated gaussian expressions.

So far we have only stated that the functions ϕ^{GF} have the exponential form of a gaussian. We now limit ourselves to functions having the symmetry of atomic orbitals. This gives us for example

$$\begin{aligned} g_{1s} &= (8\alpha^3/\pi^3)^{1/4}e^{-\alpha r^2} \\ g_{2p_x} &= (128\alpha^5/\pi^3)^{1/4}xe^{-\alpha r^2} \\ g_{3d_{xy}} &= (2048\alpha^7/\pi^3)^{1/4}xye^{-\alpha r^2} \end{aligned} \tag{2.35}$$

The 2s, 3p etc. functions do not have the same desirable properties for integral evaluation as the 1s, 2p etc and hence, all functions of s symmetry are expanded in terms of 1s gaussians, all p functions in terms of 2p gaussians etc. These are the primitive functions that will be used in the linear expansion (2.34).

The simplest basis sets consist of the smallest possible number of functions per atom necessary to describe the occupied atomic orbitals-a so called minimal basis set. Of these, the most widely used has been the STO-3G set which uses a slater type function to describe each atomic orbital. This is then modeled by an expansion of three gaussian functions. One further simplification occurs in the use of the same exponents for the expansion of the 2s and 2p orbitals. This results in both functions having the same radial form and hence only one radial integration is necessary for the given sp shell. Improvements to the set are generated by increasing the contraction length of the expansion giving rise to STO-4G, STO-5G etc sets which use four and five gaussian respectively to model the desired slater type function. However, it has been shown empirically that STO-3G is sufficient to reproduce essentially all the valence behaviour of a slater orbital calculation.

Obviously, STO-3G is not the only possible minimal basis set. Huzinaga has generated basis sets by a combined process of energy minimization and fitting to results of numerical Hartree-Fock calculations on atoms, leading to an optimum set of exponents and expansion coefficients [30]. Since these sets are available for

all the elements upto Z=86 and provide a valence shell description better than split valence STO type sets (discussed latter), they have been used throughout most of my work

The next stage in sophistication is provided by allowing the size of the valence orbitals to either expand or contract during the course of the calculation. This is achieved through the use of split valence basis sets which contain a description of two different valence orbitals. Usually, one is chosen to be slightly larger than the true valence orbital, and the other slightly smaller. Hence, the variational principle will select the optimum mixture of the two functions (and hence the size of the valence shell) during the iterative cycle. We now have the notation 4-31G (for example) which means that the core orbitals are expressed as a contraction of 4 gaussians, while the valence orbitals have been split into two, with one having a contraction length of three and the other being an uncontracted primitive gaussian. This process can be continued to give sets in which the valence orbitals are split into three or more parts.

The finally level of sophistication is to allow the shape of the valence orbitals to deform. This is achieved by adding a function of higher angular momentum (i.e. a p function to H, a d function to the first row etc.) called a polarization function. This function now allows a hybridised orbital of higher angular momentum to be formed which can deform under an external field (such as one finds in molecules).

The polarization function usually consists of a single primitive gaussian. It has been shown empirically, that the addition of polarization functions is more important for heavy atoms, and this generates a set with the notation 4-31G* (for example). If p functions are added to the hydrogen as well as d functions to the first row atoms we arrive at 4-31G** (for example). Again, this can be continued by adding several polarization functions, f type functions to heavier atoms etc.

However, since most of my work has involved relatively heavy atoms (first transition period), we have restricted ourselves to the use of minimal basis sets; in particular, those due to Huzinaga. This is because more sophisticated approaches lead to prohibitively large run times and storage requirements (the number of two electron integrals to be evaluated scales as the fourth power of the number of basis functions). While an improvement in basis set may lead to an improvement in the quality of the results, it seems unlikely that the overall conclusions will be significantly changed since a wealth of previous calculations show that minimal basis sets yield very good results when used in geometry optimisation calculations [31].

2.4 The GAMESS SCF-MO Program

A landmark in quantum chemistry occurred with the publication of the GAUSSIAN [32] suite of programs which provided one of the first freely available im-

plementations of the Hartree-Fock method using, as the name implies, gaussian basis functions. However, the package suffers from the severe drawback of making no use of molecular symmetry which can obviously greatly reduce computational cost.

This drawback has been overcome in the GAMESS (Generalized Atomic and Molecular Electronic Structure Systems) package by Guest and Kendrick [33] which shares many of the features of the GAUSSIAN program but takes full account of available symmetry. Because of this advantage, much of my research has been conducted using this program.

The basic SCF procedure is illustrated if figure 2.1. Input to the program is via a Z matrix specifying internal coordinates in terms of bond lengths and angles (figure 2.2) together with a basis set-either one of the standard internal sets or through the external specification of the exponents and contraction coefficients.

Obviously, most iterative processes will not converge without assistance, and to this end a variety of convergence aids are also available. The most useful of these is the level shifter method of Saunders and Hillier [34] which basically ensures diagonal dominance of the matrix at each cycle.

The output consists of the converged total energy, together with the final molecular orbitals and an analysis of the charge distribution generated using Mulliken population analysis.

1) Specification of initial molecular geometry.

2) Calculate symmetry information.

3) Calculate required integrals ($S_{\nu\mu}, H^{core}_{\nu\mu}, (\nu\mu \mid \lambda\sigma)$).

4) Calculate starting guess at **P**, the density matrix.

5) Calculate **G** from the density matrix and two electron integrals (2.28),(2.29).

6) Add **G** to $\mathbf{H}^{core}$ to obtain the Fock matrix (2.28)

7) Solve generalised eigenvalue problem to obtain **C** and ϵ.

8) Calculate new density matrix from **C** (2.25).

9) Check for convergence by comparing the new density matrix with the old one. If the procedure has not converged, return to step 5.

10) Output required properties.

Figure 2.1 The SCF Iterative Cycle

Atom Type	Atom to Which it is Bonded	Internuclear Distance	2nd Centre for Angular Specification	Nuclear Angle
O				
H	1	OH		
H	1	OH	2	HOH

The above z-matrix refers to a water molecule of the form

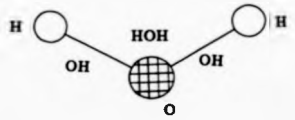

Figure 2.2 Z-Matrix for Water

Although geometry optimisation routines are provided, these perform an analytic evaluation of the energy gradients which is very time consuming. Therefore, we search the desired parameter space by a process of trial and error, and then determine the minimum energy configuration by a process of curve fitting. While slightly less accurate, this procedure is very much quicker when large systems are under investigation.

2.5 Problems and Extensions

The restricted Hartree-Fock method suffers from two major failings. Firstly, problems arise when considering the dissociation of molecules whose bonds cleave homolytically (i.e. $H_2 \rightarrow H + H$). Due to the constraint of double occupancy of the molecular orbitals, the RHF method will give wrong dissociation products ($H_2 \rightarrow H^+ + H^-$). Fortunately, my research deals with equilibrium geometries where this type of process is unimportant.

This problem also leads to difficulties in the calculation of binding energies. Ideally, we would calculate the minimum energy for the surface atoms and the adsorbate, and then subtract off a reference energy consisting of the energy of the surface atoms alone and the adsorbate alone. The generation of this reference level leads to complications. We cannot simply remove the adsorbate to large distances and perform a single calculation (usually) because of the dissociation problem

mentioned above. Also, since the method is variational, it is necessary to include the empty or ghost orbitals of the adsorbate when calculating the energy of the surface alone, and the ghost orbitals of the surface when calculating the energy of the adsorbate alone in order to maintain a consistent number of degrees of freedom throughout. Unfortunately, the GAMESS package does not allow the placement of ghost orbitals on dummy centres and hence we have not generally been able to calculate binding energies. Fortunately, we are not interested in calculating binding energies, and hence this drawback is of little consequence.

Secondly, the Hartree-Fock method neglects the effects of electron-electron correlation. (Although, due to the determinental nature of the wavefunction, correlation effects between electrons of the same spin are included-e.g. Pauli's exclusion principle is obeyed). Fortunately, for geometry calculations correlation effects are relatively unimportant. While the inclusion of correlation effects will obviously alter the absolute value of the minimum energy, they do not generally alter the optimum geometry by any great amount .(i.e. The calculated potential energy surface is nearly parallel to the true surface in the vast majority of cases). However, if desired various methods of including these effects exist.

The most common approach is via configuration interaction (CI) [35,36]. As the result of an HF calculation, we are left with a single slater determinant constructed from a set of occupied orbitals and a set of unoccupied, or virtual, orbitals. CI

uses the single slater determinant as the first term in an (infinite) expansion. The second term consists of all possible determinants constructed by replacing one of the occupied orbitals by one of the virtual orbitals. The third term contains all double replacements etc. If we start with a complete basis set and consider CI to infinite order, then we in principle, generate the exact wavefunction for the system. Obviously, this is impossible in practice. The usual approach is to truncate the expansion after double replacements, but even this limited form of CI is impractical for large systems such as the ones we have considered during the course of my work.

The main alternative to CI is some form of perturbation expansion in which the Hartree-Fock wavefunction is used as the reference level and correlation effects are added as a perturbation away from this state [37]. Again, these techniques are very time consuming in practice and cannot be used for the size of system of interest in my research. Fortunately, RHF provides a good description of equilibrium geometries, and hence, these correlation methods are of no importance in my work. (For a full review of ab initio Hartree-Fock theory as well as methods of accounting for correlation effects see [38]).

Chapter 3

Formate and Methoxy on Cu(100)

3.1 Background and Motivation

The study of alcohol chemisorption on metal surfaces is of importance both for corrosion and catalytic research. Alcohols contain reactive OH groups, which are normally split via breaking of the O-H bond upon chemisorption. Thus, they share the same bond breaking mechanism with water chemisorption, and it is possible that this, together with studies of the resultant organic fragments, may lend some insight into the mechaniams of corrosion initiation and inhibition.

The dehydrogenation of alcohols over metals is an important and well studied reaction, but little information existed at the molecular level until recently. (The motivation for these studies arises from the reverse reaction i.e. hydrogenation

of molecular fragments to produce methanol.) Methanol adsorption on metals was initially studied using UV photoemission on a wide variety of metals i.e. Pd [39], Ni(111) [40], Ru(001) [41],and W(100) [42]. All of these studies showed that methanol fragments on the surface, leaving chemisorbed carbon monoxide. However, an IR study by Byholder and Neff [43] on iron demonstrated that methanol and other alcohols form stable alkoxide surface intermediate species in which the O-H bond is broken and replaced by an O-metal bond.

Copper is a good selective catalyst in the oxidation of methanol and ethanol during conversion to aldehydes [44,45]. The initial step here is identical to the situation for iron in that the alcohol O-H bond is broken, but the C-O bond remains intact. Also, copper serves as a catalyst for the oxidation of formaldehyde to produce formic acid, and the decomposition of formic acid to carbon dioxide. In all these processes, again, the carbon-oxygen bond remains intact.

The high selectivity of these reactions is thought to be due to the formation of one or more stable intermediate species on the surface. Work by Wachs and Madix [44,45] on the oxidation of CH_3OH (and C_2H_5OH) using thermal desorption methods showed that CH_3O (and C_2H_5O) were found on the surface during the reaction. (This had earlier been proposed via analysis of IR results [46,47].)

Early EELS work on these hydrocarbons [48,49] was complicated by charge transfer between the substrate and the adsorbate, but the HREELS study of Sex-

ton [50] showed clearly that the methoxy (CH_3O) group was bonded to the surface via the oxygen end. Use of the dipole selection rule showed that, furthermore, the molecule was orientated normal to the surface. Further EELS work by Andersson and Persson [51] compared the observed symmetry of the surface phonons with the symmetry of the available surface sites, and concluded that the methoxy occupied the four fold hollow positions. This conclusion was supported by Paul and Rosen [52] who, by comparison of the observed and calculated ionization potentials, also proposed a four fold hollow site. Early NEXAFS work by Stohr et al [53] gave an untilted methoxy, but could not assign a site to the group. Finally, Ryberg [54] used IRS and showed in contrast to previous studies that, assuming occupation of the four fold hollow site, the methoxy group was tilted with respect to the surface normal.

In the case of formaldehyde and formic acid reactions on copper, it was thought that the formate (HCOO) group played a similar role to the much studied methoxy group in methanol reactions, and was the intermediate species responsible for the selectivity of these reactions.

The importance of these two intermediates in the catalytic production of basic hydrocarbon molecules made them ideal candidates for study using the relatively new techniques of SEXAFS and NEXAFS.

3.2 SEXAFS and NEXAFS Results.

Outka et al [7] performed experiments on both formate and methoxy on Cu(100). For formate, they proposed a bridge site in which the oxygen atoms sit near the four fold hollow positions (fig 3.1a). This leads to anomalous copper-oxygen bonds of $2.38\AA$ (an average of two bonds of lengths $2.13\AA$ and $2.45\AA$ created by the mismatch between the oxygen-oxygen and copper-copper bond lengths resulting in the oxygens being off centre from the four fold hollow site.) This is nearly $0.4\AA$ greater than normal Cu-O bonds which lie in the range $1.7 - 2.0\AA$ and was proposed as the first example of a molecular system that deviated from results predictable via Paulings bonding concepts [18,55,56]. Indirect support for this model was provided by Upton [57] who performed a generalized valence bond (GVB) calculation on formate on Ni(100). He optimized the bond lengths for the Outka model and found bonds about 40% longer than normal.

The results presented for methoxy were more complex, but they concluded that methoxy was tilted by $32 \pm 10°$, was definitely not in an atop site, but may be in a mixture of two fold bridge and four fold hollow sites.

Reanalysis of Outka's data on formate by Crapper et al [8,58-60] using a multishell simulation technique rather than the direct fourier transformation method showed that Outka's model was unacceptable, and instead proposed an atop configuration with the oxygens directed towards the four fold hollow sites (fig 3.1b).

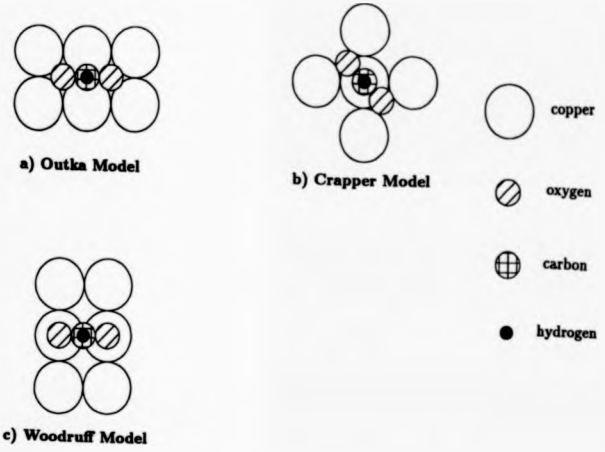

Figure 3.1. Models of Formate on Cu(100)

This gave a more normal bond length of 1.99$\AA$. Finally, photoelectron work by Woodruff et al [9] proposed yet another site. This work favoured a bridge configuration with the oxygen atoms lying virtually above the copper atoms (fig 3.1c). This model also gave a reasonable fit to the EXAFS data, and hence must be thought of as the most likely candidate from the mass of experimental data.

Finally, a photoelectron diffraction study by Kilcoyne et al [61] on methoxy on Cu(100) appears to favour a low symmetry site for this group situated about one third of the way from the four fold hollow to the two fold bridge site with the methoxy being untilted.

The confused situation produced by the analysis of all the experimental data on these two related organic systems provided an ideal situation for an initial use of our cluster methods.

3.3 Results

3.3.1 Formate on Cu(100)

The argument over this structure was centred around the choice between Outka et al's four fold hollow site with the anomalous copper-oxygen bond length and Woodruff et al's bridge site, which is indicated by photoelectron work and also provides a relatively good fit to the multishell EXAFS analysis.

We therefore decided to perform a restricted Hartree-Fock calculation using the GAMESS program to try to distinguish between these two sites. Minimal basis sets due to Huzinaga [62] were used throughout.

However, as a preliminary test of the accuracy of the predictive capabilities of the program and the basis sets, we began by optimising the geometry of a copper formate molecule. Experimental data for this system is available through the work of Barclay and Kennard [63]. The structure of the formate group was held fixed at the values given by them of; C-O bond length 1.26$\AA$, O-C-O angle of 125.5° and C-H bond length of 1.07$\AA$ and the copper oxygen bond length was optimised by energy minimisation. This resulted in a calculated bond length of 2.01$\AA$, in excellent agreement with the experimental value of 2.02$\AA$.

The main calculations were performed on a Cu_8 cluster (fig 3.2) which allows both the Outka and the Woodruff model to be examined. Hence, the calculated minimum energies are directly comparable without the need to subtract background reference levels. The eight copper atoms were held invariant at the positions of a bulk terminated (100) copper surface throughout.

The formate structure was also held fixed with the structural parameters being those given by Barclay and Kennard [63]. Optimisation of the formate structure would obviously lead to a refinement of the results but should not alter the overall conclusions provided that the energy difference between the two sites is sufficiently

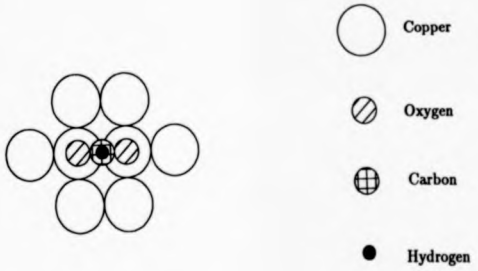

Figure 3.2 The Cu_6 Cluster

large. Also, such an optimisation would greatly increase the complexity of the calculation due to the large number of extra variables it would introduce into the optimisation scheme. Having defined the surface and formate structures we then optimised the vertical distance of the formate group above the copper surface by minimising the total energy with respect to this parameter.

For the Outka model we found a minimum energy structure corresponding to a Cu-O bond length of $2.32\AA$ in excellent agreement with the experimental bond length of $2.38 \pm 0.03\AA$ [7]. For the Woodruff model agreement is again good with the calculated bond length of $1.90\AA$ agreeing well with the experimental value of $1.98 \pm 0.04\AA$ [9]. However, the energy of the Woodruff model was 0.38eV lower than that of the Outka model. Thus, the Woodruff model is significantly more stable than the Outka model and must be considered as by far the more likely to be correct. It must be regarded as a coincidence that the bond length calculated for the Outka model agreed so well with the experimental value.

Two questions still need to be addressed: convergence of the results with respect to cluster size and basis set size. In order to establish convergence with respect to cluster size we performed calculations using clusters of two, six and eight copper atoms. In each case the bond lengths and energy differences between the two structures were in close agreement showing that the eight atom cluster is sufficient for convergence.

Convergence with respect to basis set size could not be established since we had insufficient storage available to move beyond the minimal basis set level. However, the results for the copper formate molecule appears to show that Huzinaga sets are sufficient for good agreement in the case of this system. Moving beyond minimal basis sets may lead to a refinement in the calculated values but should not alter the overall conclusions.

3.3.2 Methoxy on Cu(100)

In the case of methoxy, the choice of sites is more complex with only the atop site having been ruled out by experimental studies. We therefore have to choose between the two fold bridge site, the four fold hollow site and Kilcoyne's asymmetric site between the hollow and bridge sites.

As before, a restricted Hartree-Fock calculation using the GAMESS program and minimal basis sets due to Huzinaga were employed. We calculated the energy of a cluster representing the methoxy on Cu(100) as a function of displacement of the methoxy group along a line joining the bridge and the hollow sites. At each such displacement we minimised the energy with respect to the normal distance between the surface and the oxygen atom of the methoxy group. This process covers all the previously proposed sites. Having located the minimum energy site, we then calculated the energy as a function of the methoxy tilt angle in order to

address the question of whether or not the group is normal to the surface.

In order to look at convergence with respect to cluster size, we calculated the energy of the Cu_6, Cu_8, and Cu_9 clusters shown in figure 3.3. The corresponding energy functions for displacements are shown in figure 3.4. The Cu_6 cluster is clearly inadequate since the addition of two second layer copper atoms shifts the location of the energy minimum from close to Kilcoyne's asymmetric site to the four fold hollow site. The nine copper atom cluster results closely agree with the results for the eight atom cluster which we therefore propose is adequate for these calculations.

The energy function has two minima at the hollow and bridge sites with the hollow site being some 0.11eV lower in energy. Hence, at equilibrium the hollow site would be far more densely populated at room temperature. However, the potential barrier of 0.05eV between the two sites could retard the approach to equilibrium and result in a non-equilibrium mixed phase being observed experimentally as proposed by Outka et al [7]. Figure 3.5 shows the energy as a function of the tilt angle between the surface normal and the oxygen-carbon bond for the methoxy in the four fold hollow site with the tilt being in the plane normal to the surface and passing through the bridge and hollow sites. The energy increases monotonically with tilt angle and hence we conclude that the methoxy is untilted. Rotation of the three hydrogen atoms about the O-C axis results in changes of

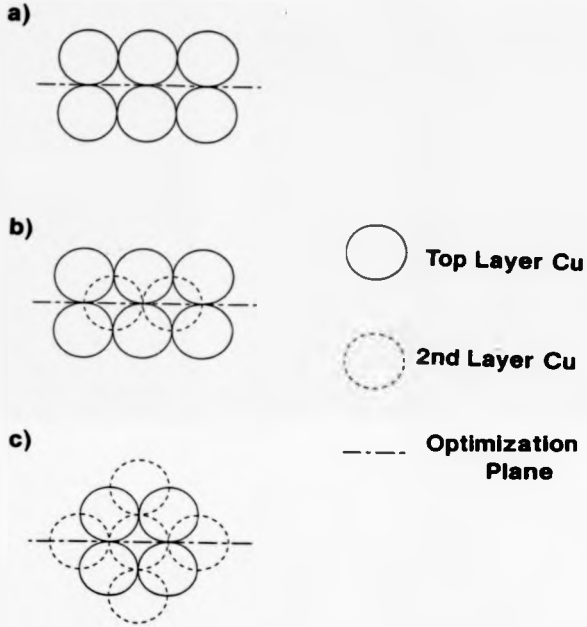

Figure 3.3 The Cu_4, Cu_6 and Cu_9 Clusters used in the Methoxy Calculations

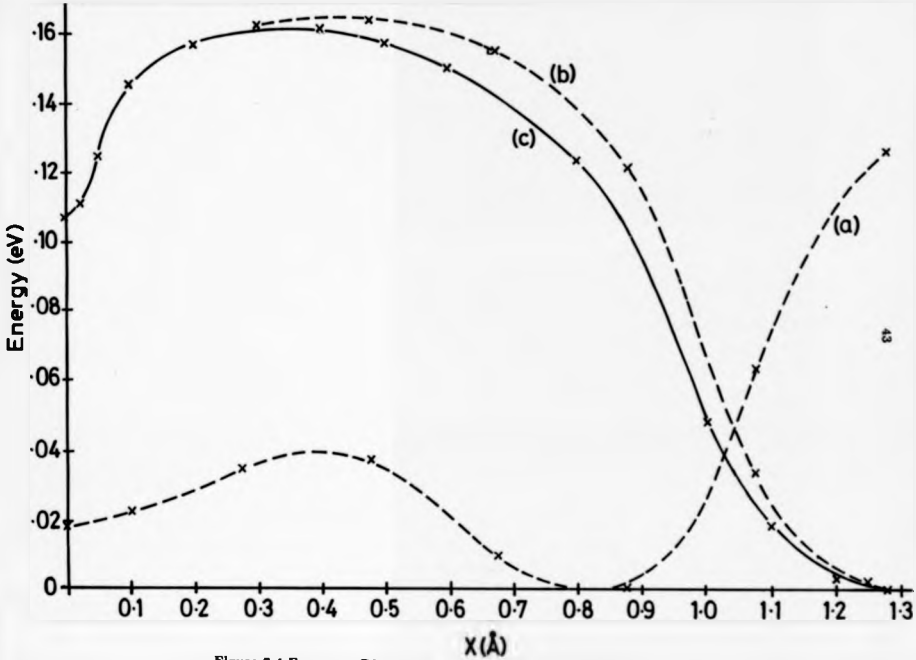

Figure 3.4 Energy v. Distance for a) Cu_2 Cluster b)Cu_3 Cluster

less than 0.01eV in the energy.

We therefore conclude that the methoxy group is vertical and occupies a mixture of bridge and hollow sites on the Cu(100) surface with occupation of the hollow site being much greater than the occupation of the bridge site. We find the copper-oxygen bond length to be $1.99\AA$.

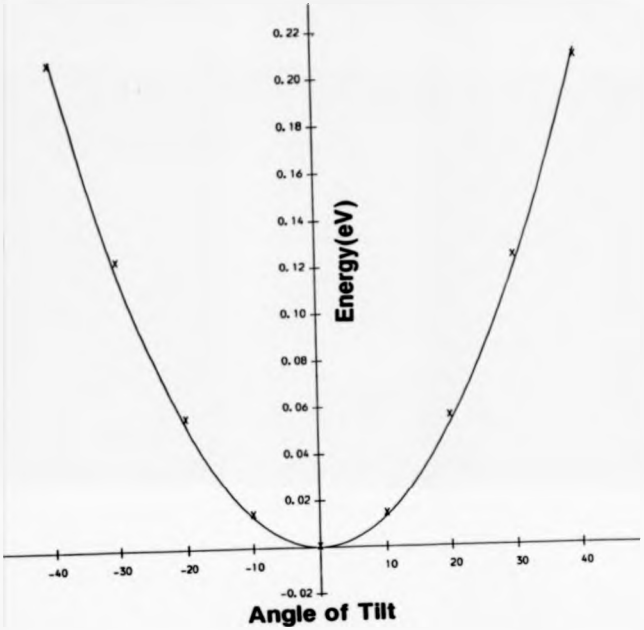

Figure 3.5 Energy v. Tilt Angle for Methoxy

Chapter 4

The Low Temperature Structure of Oxygen on Cu(110)

4.1 Background and Motivation

While the high temperature ordered structure of oxygen on Cu(110) has been extensively studied, the low temperature disordered phase has, until recently, received little attention. Now however, two experiments have been performed which have yielded conflicting evidence.

The initial study by Prabhakaran et al [12,64] used UPS, XPS, AES, HREELS and LEED to conclude that the adsorption process was molecular in nature. A variety of evidence was presented to support this view. Firstly, the UPS signal they

observed showed a three peaked structure that was thought to be a characteristic of molecular oxygen [65,66]. This feature was also seen in an early UPS study of this system performed by Spitzer and Luth [67,68]. Also, they observed an XPS signal from the O(1s) level of molecular O_2 at 533.5eV.

Further evidence came from the HREELS results. These showed a prominent signal at 660cm^{-1} which they ascribed to an oxygen-oxygen stretch mode due to it's similar frequency to that observed for molecular oxygen on Ag and Pt surfaces [69,70]. Finally, an AES signal observed at 520eV was assigned to a molecular oxygen transition.

All of these signals disappeared on annealing the surface to 150K which was therefore postulated to be the oxygen dissociation temperature on this surface.

However, a subsequent study by Mundenar et al [13,71] presents contradictory results. They again employed HREELS and UPS to study the low temperature structure of oxygen on Cu(110). They find no evidence of an EELS signal that can be assigned to an oxygen-oxygen stretch mode, and find only an oxygen-metal vibrational mode centred on 49meV, in agreement with the earlier EELS work of Wendelken [72].

They also show that the three peaked UPS signal may be due to small amounts of an impurity (either H_2O or CO) coadsorbed on an oxygen predosed surface. This effect had earlier been proposed by Prince and Paolucci [73]. Carbon monoxide

adsorption on copper should be recognizable by a set of satellite peaks around the valence band UPS signal [74], which was not observed by Prabhakaran. However, as pointed out by Kanski et al [75], this characteristic fingerprint may be absent when CO is coadsorbed with oxygen, and hence, the presence of CO may have been missed by the earlier workers.

Uptake data from Mundenar et al's work also showed that the process must be dissociative with at most small areas of molecular oxygen forming isolated islands on the surface. The XPS signal reported by Prabhakaran was only observed by Mundenar after exposure of the oxygen covered surface to small amounts of H_2O. The AES signal attributed to an O_2 transition has also been observed at room temperature where the oxygen is definitely atomic and hence this signal cannot be due to a molecular transition.

Finally, Mundenar proposes that the HREELS signal assigned to the O-O stretch mode by Prabhakaran could be due to a hindered libration of H_2O on the surface as observed by Sexton [76].

However, these conclusions by Mundenar et al have been hotly disputed by Prabhakaran et al and the situation remains confused. In particular, the disappearance of the signals ascribed to molecular oxygen at 150K seems problematic since both H_2O and CO should be liberated at much higher temperatures. However, it should be remembered that the presence of oxygen as well as the impurity

may result in a lowering of the liberation temperature.

Hence, the structure remains in doubt and the choice between molecular and atomic oxygen remains an open one although the evidence in favour of atomic oxygen seems much stronger. In an attempt to shed some light on the confused situation, we decided to apply the techniques which had been successful in the case of formate and methoxy on Cu(100) to this problem.

4.2 Results

We again employed the restricted Hartree-Fock method as implemented in the GAMESS package together with minimal basis sets due to Huzinaga throughout the calculations. However, no sites had been suggested for this system and hence, all high symmetry sites on the (110) surface were investigated (fig 4.1a).

A Cu_{12} cluster (fig 4.1b) was chosen for the calculations, which is large enough to allow all the high symmetry sites to be investigated on the same cluster. Hence, total energies are directly comparable without the need to subtract background reference levels. The twelve copper atoms were held fixed in the positions of an unrelaxed Cu(110) surface throughout. The vertical distance of the adsorbate from the cluster was then optimized by minimising the total energy with respect to this variable.

For molecular oxygen, the oxygen-oxygen bond was held fixed at the free

a)

b)

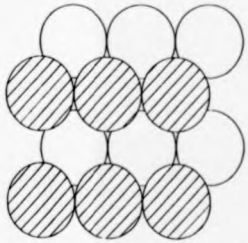

Figure 4.1 a) High Symmetry Sites on Cu(110)
b) The Cu_{12} Cluster

molecule value of 1.206$\AA$ and the calculations were repeated with the O-O axis both parallel to and perpendicular to the copper surface. For the parallel case, a number of different sites are available generated by rotations of the oxygen molecule about the surface normal through angles of 0°, 45° and 90° (fig 4.2). No evidence of a stable structure involving O_2 chemisorption has been found on this surface. Hence, there appears to be no evidence to support the molecular viewpoint of Prabhakaran et al.

For atomic oxygen stable configurations where found in all the high symmetry sites although the most stable by far is the long bridge site in which the oxygen atom forms Cu-O bonds of 1.8$\AA$ with both the first and second layer Cu atoms. Table 4.1 summarises the relative stability of atomic oxygen in all the high symmetry sites.

The energy of the vibrational mode was then calculated by generating the potential energy curve given by vertical displacements of the oxygen atom about the equilibrium position. (The frozen phonon approximation). During this process the copper atoms were held invariant. This mode was found to have an energy of 52.9meV, in excellent agreement with the experimental value of 49meV given by Mundenar et al.

In conclusion, we fully support the atomic chemisorption process proposed by Mundenar et al and postulate that the oxygen atom occupies the long bridge site

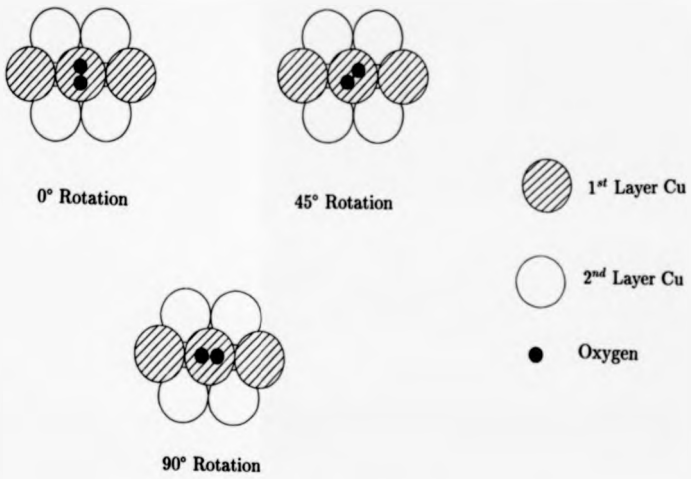

Figure 4.2 Illustration of Rotations of Molecular Oxygen on Cu(110)

Site	Bond Length (Å)	Relative Energy (eV)
Short Bridge	1.8	+0.55
Long Bridge	1.8	0.0
Atop 1st layer	1.8	+1.20
Atop 2nd layer	1.7/2.0[a]	+0.21

Table 4.1 Summary of Atomic Adsorption Parameters

[a] 1.7Å with 2nd layer, 2.0Å with 1st layer.

on the Cu(110) surface at low temperatures.

Chapter 5

Oxidation of Si(100)

5.1 Background and Motivation

The chemisorption of oxygen on semiconductor surfaces has been the subject of extensive research [4]. This has been motivated both by the technological importance of the process to the semiconductor industry and by a desire to achieve a fundamental understanding of such effects. Unfortunately, the chemisorption of oxygen on silicon surfaces has led to controversy over whether the process is molecular or atomic in nature [4,77-81]. Some studies have stated that the adsorption process depends on the experimental conditions, and both atomic and molecular oxygen may be present on the surface simultaneously [82-84]. However, recent work favours an atomic process (at least initially) [81,85-87]. Theoretical studies

have been more straightforward with virtually all of them supporting the atomic viewpoint [78-80,88-93].

Keim et al [77] managed to differentiate between the two processes on Si(100) by performing experiments with O_2 and N_2O (which readily dissociates into N_2 and O). This work together with that of Ibach et al [81] and Schaefer et al [86,87] shows that, at low exposures, each O_2 molecule dissociates on Si(100) with one O atom being adsorbed at the dimer bridge site while the other goes into the Si-Si backbond. At higher coverages (0.5 to 1.0 monolayers of oxygen) the situation becomes more confused with oxygen being adsorbed into the subsurface lattice. With N_2O, the situation is much simpler with oxygen only being adsorbed at the dimer bridge sites.

The N_2O results are consistent with the theoretical work of Barone et al [78,79,93] and Batra et al [80] on the adsorption of atomic oxygen. They used MNDO and MCSCF cluster models respectively to show that atomic oxygen is most stable in the bridge sites on the bulk terminated Si(100) surface and that the oxygen atom lies within 0.05-0.25$\AA$ of the surface plane.

However, all of these calculations have been performed on clusters that neglect the effects of surface reconstruction. Both theoretical [15,94] and STM [95,96] studies have shown that Si(100) undergoes a large scale reconstruction in which adjacent silicon atoms bond together to form 2×1 domains of symmetric dimers.

We therefore decided to repeat the earlier theoretical studies taking full account of this reconstruction. All our calculations were performed using the GAMESS package [33] at the restricted Hartree-Fock level.

5.2 Dimer and Non-Dimer Bridge Sites

The 2×1 reconstruction leads to three inequivalent bridge sites on the Si(100) surface; the dimer bridge site, the non-dimer bridge site and the transverse bridge site (fig 5.1). Previous work [78,79] has shown that the binding energy for the transverse bridge site is significantly lower than that of the other two sites because of the orientation of the surface Si dangling bonds and we therefore restrict ourselves to studies of the dimer and non-dimer bridge sites.

The relative stabilities of these two sites was investigated using the $Si_{18}H_{24}$-O cluster (fig 5.2), and the minimal STO-3G basis set. The first set of calculations determined the energy of an oxygen atom at a non-dimer bridge site as a function of the tilt angle θ. All the sub-surface silicon atoms were held invariant, and all Si-Si bond lengths were held fixed at the bulk Si-Si distance of $2.352\mathring{A}$, thus defining ϕ as a function of θ. The minimum energy configuration corresponds to a tilt of 20.74° (compared to 33.24° for the symmetric dimer) with the oxygen being $0.792\mathring{A}$ above the silicon atom to which it is bonded.

The second set of calculations used the same cluster and basis set, with the

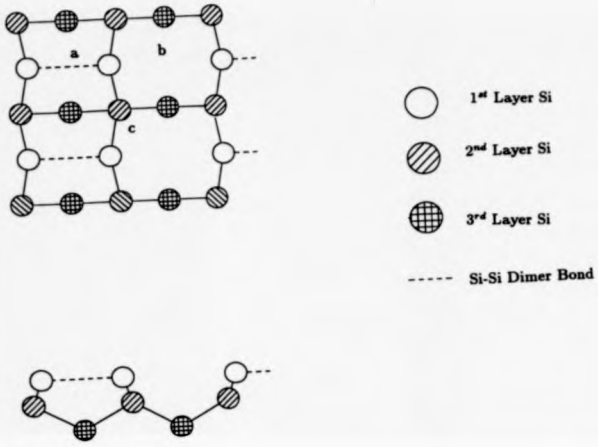

Figure 5.1 Bonding Sites on Si(100)(2×1)

a) Dimer Bridge Site

b) Non-Dimer Bridge Site

c) Tranverse Bridge Site

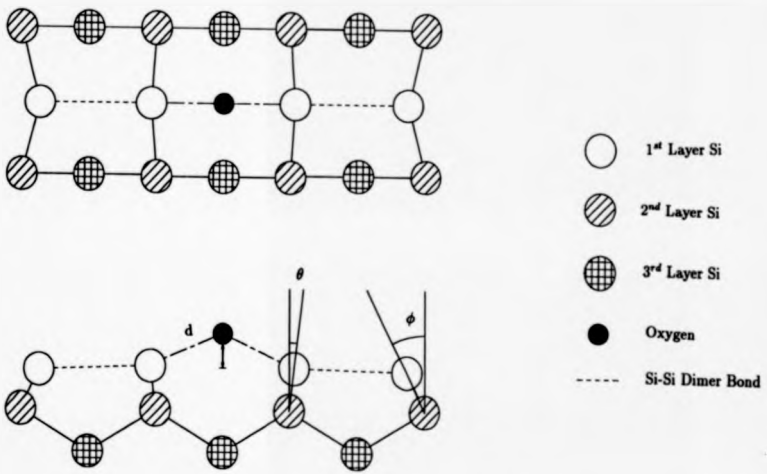

Figure 5.2 $Si_{18}H_{24}$-O Cluster. (The H atoms have been omitted for clarity)

oxygen atom this time occupying the dimer bridge site between the two silicon atoms at the right of the cluster. To simulate a symmetric dimer, we set $\theta = \phi$ and then vary θ in order to locate the minimum energy configuration. In order to simulate the 2×1 dimer structure, the geometry at the left of the cluster was taken to be that of an undistorted dimer with $\theta = 33.24°$. The minimum energy this time occurs at an angle of 12.5°, with the oxygen atom sitting $0.048\mathring{A}$ below the silicon surface giving an Si-O bond length of $1.627\mathring{A}$. The significant fact was that the energy of the dimer bridge site was found to be some 5.56eV lower than the non-dimer bridge site configuration, and hence we conclude that in the initial stages, chemisorption occurs at the dimer bridge site.

5.3 The Dimer Bridge Site

We now turned to consider convergence of the results with respect to both cluster and basis set size. In order to investigate convergence with cluster size we employed the $Si_{18}H_{28}$-O cluster (fig 5.3) and the Si_9H_{12}-O cluster which is generated by truncating the $Si_{18}H_{28}$-O cluster to the central region. As previously, we optimised the oxygen dimer bridge position as a function of θ keeping the other atoms invariant. For the large cluster, the calculations were tried with the outer silicons vertical (simulating the unreconstructed surface) and tilted at 33.24° and saturated with a hydrogen atom to simulate the 2×1 reconstructed surface. These

configurations yielded virtually identical results. Figure 5.4 shows the variation of E_{TOT} and R as a function of θ for these two clusters, with the energy being defined relative to the clean 2×1 surface. Obviously, the results are very similar, with R varying by less than $0.02\AA$ and E_{TOT} by less than 0.2eV over the entire range of θ. In agreement with section 5.2, the oxygen atom is found to lie about $0.05\AA$ below the silicon surface with the Si-Si surface to sub-surface bond being tilted by about 13° with respect to the surface normal, the associated Si-O bond length being about $1.62\AA$. (Table 5.1 summarises these results).

Clearly, these results show that the small Si_9H_{12}-O cluster is perfectly adequate for studying the adsorption process and show that the results are fully convergent with respect to cluster size.

To investigate the convergence with respect to basis set size we repeated the above calculations using the split valence 3-21G basis set of Pople [97] and a Huzinaga minimal basis set [62]. While these two sets are still relatively simple, they should be sufficient to demonstrate whether or not a drastic alteration of the calculated properties would be generated by moving beyond the simple basis set level. The results obtained for the Si_9H_{12}-O cluster using these two sets are also displayed in table 5.1. The Huzinaga set gives a double minima with the two minimum energy configurations being separated by a barrier of only 0.007eV. Hence, we are unable to specify a unique value for R or a meaningful vibrational

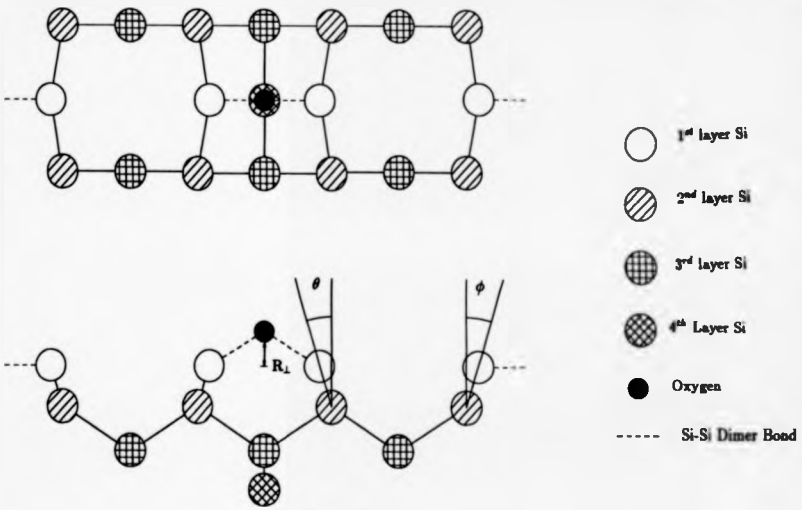

Figure 5.3 $Si_{19}H_{26}$-O Cluster

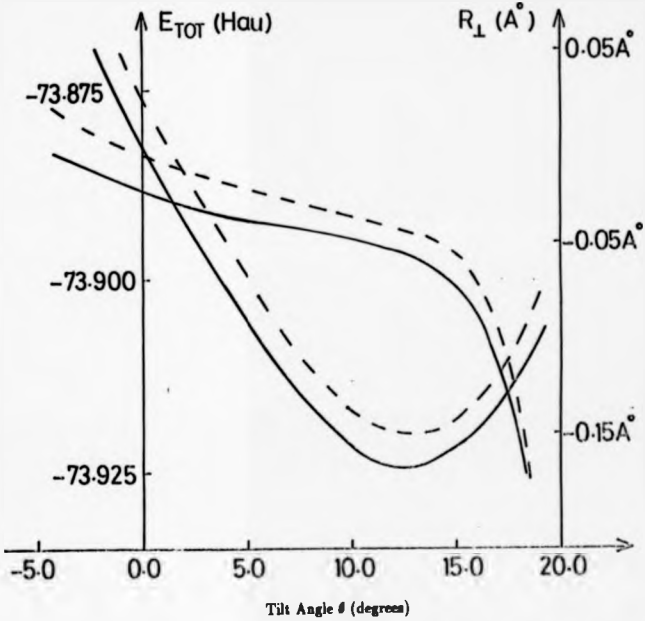

Figure 5.4. E_{TOT} and $R_\perp$ v. θ

Cluster	Basis Set	θ	$R_\perp(\AA)$	$d_{Si-O}(\AA)$	$\omega(cm^{-1})$
$Si_{18}H_{28}$-O	STO-3G	12.5	-0.048	1.627	366
$Si_{19}H_{28}$-O	STO-3G	13.1	-0.046	1.613	348
Si_9H_{12}-O	STO-3G	12.5	-0.057	1.627	368
Si_9H_{12}-O	SV3-21G	11.3	0.092	1.657	335
Si_9H_{12}-O	Huzinaga	12.0	0.139	1.644	-
	(333/33)		0.202	1.650	

Table 5.1 Parameter values for the chemisorption of atomic oxygen at a dimer bridge site on the Si(100) surface

frequency for this set.

The important conclusion to be drawn from table 5.1 is that all the calculations yield essentially the same geometry. The oxygen atom breaks the Si-Si dimer bond and forms a new Si-O-Si configuration with the Si-Si surface to sub-surface bond being tilted by about 12.5° with respect to the surface normal. The oxygen atom lies within $0.2\AA$ of the surface, and the Si-O bondlength is about $1.635\AA$. The calculated vibrational frequencies are also fairly consistent and in better agreement with the experimental value of $370cm^{-1}$ than the earlier theoretical prediction [80].

5.4 High Coverage

LEED studies of the oxidation of Si(100) indicate two distinct phases [77]. In the initial stages the 2×1 pattern remains clearly visible, which we interpret as the adsorption of oxygen at the dimer bridge sites as discussed in the last section. At higher coverages, the 2×1 pattern is replaced by a 1×1 pattern which becomes diffuse at still higher exposures.

One obvious way in which the transition from a 2×1 to a 1×1 topology could occur is if the growth of the oxide layer is along the $(0\bar{1}1)$ direction, and the dimer and non-dimer sites become equivalent at high coverages. In order to investigate this possibility we used the $Si_{15}H_{20}$-O_2 cluster (fig 5.5). This cluster incorporates the adsorption of an oxygen atom at both the dimer and non-dimer bridge sites. We optimised the positions of both oxygen atoms as a function of θ the tilt of all the surface Si atoms. The total energy corresponding to the optimum configuration at each θ varies quadratically and has a well defined minimum at $\theta = 0°$. At this value the two R values become identical. Hence, at high coverages the dimer and non-dimer bridge sites become equivalent, a situation that would obviously give rise to the observed 1×1 LEED pattern. In this high coverage case we find that the oxygen atoms move away from the surface and lie $0.715\mathring{A}$ above it. This compares well with the value of $0.96\mathring{A}$ calculated by Batra et al [80] using a pseudopotential slab calculation. The vibrational frequency at high coverage was

found to be 428cm^{-1}, somewhat higher than the low coverage value of 350cm^{-1} obtained in section 5.3, and hence consistent with the experimental observation that the frequency increases with increasing exposure.

Keim et al [77] have suggested that further exposure to oxygen leads to chemisorption into the transverse bridge sites giving rise to a disordered overlayer structure and hence the observed diffuse LEED pattern. Investigation of this effect requires a very large cluster and is hence impractical because of the high computational costs it would entail.

In conclusion, we have shown that the initial stages of oxidation of the Si(100) surface gives rise to a new 2×1 structure in which the oxygen atoms occupy the dimer bridge sites and the Si-Si surface to sub-surface bonds are tilted by 12.5° with respect to the surface normal. Each oxygen atom lies within 0.2$\AA$ of the surface forming Si-O bonds of about 1.635$\AA$. The vibrational frequency for this geometry was shown to be in excellent agreement with the experimental value of 370cm^{-1}, and to increase with increasing exposure again, as observed experimentally. Finally, we have provided an explanation for the experimentally observed transition from the 2×1 to the 1×1 structure by showing that at high coverages, the dimer and non-dimer bridge sites become equivalent.

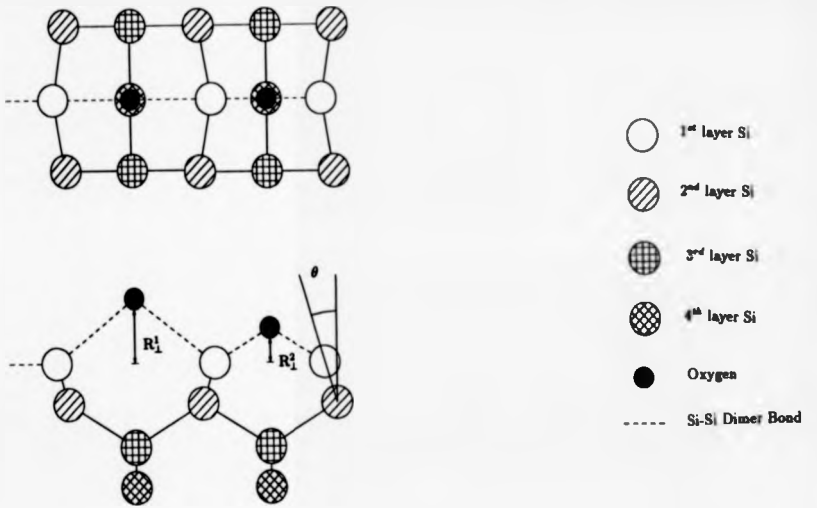

Figure 5.5. $Si_{18}H_{20}$-O_2 Cluster

Chapter 6

Semi-Empirical Methods

6.1 Background and Introduction

While the preceding three chapters have demonstrated that ab initio calculations on small clusters are capable of generating results in excellent agreement with experiment and hence are capable of use in a predictive fashion, it should be remembered that they also suffer from major drawbacks. The main difficulty in their application is the extreme demand they place on computational resources-both storage and processor time. Thus, they are only suitable for the study of the chemisorption of small molecules where small clusters can be employed with reasonable confidence. Also, it is not normally possible to progress beyond the minimal basis set level although this is not normally necessary for structural stud-

ies.

Large molecules or the study of large defects obviously demand an alternative approach. The usual choice is to turn to semi-empirical schemes in which the theory is developed to include parameters derived from experimental data. One of the most widely used schemes in the field of quantum chemistry is the extended Huckel theory (EHT) of Hoffman [98]. This method provides a good picture of the interactions between atomic orbitals but cannot be used in a predictive manner since it fails to generate reasonable bond lengths in geometry optimisations. However, as shown by Anderson [99], this failing can be corrected by the addition of a two body repulsive term. This gives rise to the atom superposition and electron delocalisation (ASED) scheme.

Atomic ionisation potentials are used as input to the calculations but isolated atom values have to be shifted by fairly large amounts to produce good results due to charge transfer between the constituent atoms of the molecule. Previous studies using ASED have performed calculations on a relevant diatomic molecule (e.g. Cu-O if studying the adsorption of oxygen on copper) and have then adjusted the ionisation potentials of the more electronegative atom in an ad hoc manner until the calculations predict charge transfers in agreement with Pauling's electronegativity theorem [18]. The atomic basis functions have then also been adjusted in order to obtain a realistic bond length for the diatomic, and the re-

sultant parameters have then been used as input to the full ASED calculations [100].

A superior treatment would include the requirements of charge self consistency in the ionisation potentials and it was hoped that this more rigorous formalism might also remove the need for shifts in the atomic orbital exponents. We therefore developed such a theory following Harrison [101] and applied it to problems of semiconductor surface reconstructions.

6.2 EHT and the ASED Scheme

In chapter 2 it was shown that minimisation of the energy of a single slater determinant using the variational principle led to a generalised matrix eigenvalue problem of the form

$$\mathbf{HC} = \mathbf{SCE} \tag{6.1}$$

where **H** is the Hamiltonian matrix, **C** is the matrix of the molecular orbital expansion coefficients, **S** is the overlap matrix and **E** is the eigenvalue matrix. Extended Huckel theory starts from this equation and constructs the Hamiltonian in a parameterised form. The diagonal elements H_{rr} can be identified with the negative of the atomic ionisation energies using Koopmans theorem [6], while the off diagonal elements are constructed as follows. Obviously, the stronger the

corresponding diagonal elements are, the stronger the off diagonal element should be and hence we let H_{ij} be proportional to the average of the diagonal elements $(H_{ii} + H_{jj})/2$. Similarly, the strength of the off diagonal interaction should decay as the size of the overlap between the corresponding atomic orbitals falls and we therefore assign

$$H_{ij} = K(H_{ii} + H_{jj})S_{ij}/2 \tag{6.2}$$

where K is the constant of proportionality and is called the Wolfsberg-Helmholtz constant. Thus, although we still have the overlap matrix to evaluate, we have circumvented the need to evaluate the time consuming two electron integrals.

We now evaluate the total energy as the sum of the one electron energies ε_i. However,

$$\sum_i \varepsilon_i = E_{en} + 2E_{ee} \tag{6.3}$$

where E_{en} is the electron-ion energy and E_{ee} is the electron-electron energy. Obviously, E_{TOT} should be given by

$$E_{TOT} = E_{en} + E_{ee} + E_{ii} \tag{6.4}$$

where E_{ii} is the ion-ion energy. We proceed by defining a repulsive correction energy E_R given by

$$E_R = E_{ii} - E_{en} \tag{6.5}$$

E_{ii} is easily calculated as a coulomb sum over point ions while we approximate

E_{ss} in the following manner.

Consider the cluster to be a superposition of rigid, undistorted atomic valence charge densities. Assuming no overlap between the charge clouds we may write the coulomb energy of a pair of atoms a and b as

$$Z_b \int \rho_a(\underline{r}) \mid \underline{r} - \underline{R}_b \mid^{-1} d^3\underline{r} \tag{6.6}$$

where Z_b is the number of valence electrons on atom b, ρ_a is the valence charge density of atom a and $\underline{R}_b$ is the position vector of atom b. (This follows directly from Gauss's law.) We now assume that this expression is valid even when overlap occurs. This has been found empirically to be a better approximation when a is the more electronegative atom of the pair. We can now evaluate E_{ss} as the sum of all such terms over all pairs of atoms in the cluster giving

$$E_{TOT} = \sum \epsilon_i + E_R \tag{6.7}$$

where

$$E_R = \sum_a \sum_{b>a} [Z_a Z_b \mid \underline{R}_b - \underline{R}_a \mid^{-1} - Z_b \int \rho_a(\underline{r}) \mid \underline{r} - \underline{R}_a \mid^{-1}] d^3\underline{r} \tag{6.8}$$

which agrees with the derivation given by Anderson [99] who made use of the Hellmann-Feynman force theorem.

We now proceed by introducing a crude form of charge self-consistency into the method. Having solved the EHT equations once, Mulliken population analysis is used to evaluate the charge shift on each atom; say δQ_a for the a^{th} atom.

Following Harrison [101], the term values of the a^{th} atom are increased by

$$\Delta I_a = (U_a + \sum_{b \neq a} \delta Q_b \mid \underline{R}_b - \underline{R}_a \mid^{-1}) \delta Q_a \qquad (6.9)$$

where U_a is the difference between the ionisation potential and the electron affinity of atom a. The first term accounts for the intra atomic effects while the second term accounts for the inter atomic effects. The long range nature of this coulomb sum forces the replacement of this finite term over the atoms of the cluster by an infinite sum over the atoms of the ideal surface as discussed by Dwyer et al [102]. The process is then iterated using Anderson's mixing scheme [103] to improve convergence until self-consistency is achieved.

6.3 Tests of the Method

Problems in semiconductor surface reconstructions have been studied using a variety of methods ranging from empirical tight binding without [16,104] and with [102] charge self consistency, to the fully charge self consistent density functional calculations of Pandey [105]. We therefore used this large database of results to test our method. Firstly, we examined the Si(111)(2×1) reconstruction using the cluster shown in figure 6.1a. Dangling hybrids were, as usual in semiconductor studies, saturated with hydrogen atoms. Atoms a and b were allowed to move independently in the (111) direction, and gaussian basis sets due to Huzinaga [62]

were used throughout.

Table 6.1 shows that the non-self-consistent ASED method correctly predicts an unbuckled dimer structure with relaxation towards the bulk. This is in agreement with the sophisticated calculations of Pandey [105] and in contrast to other non-self consistent results although the magnitude of the relaxation is over estimated.

Secondly, we examined the more ionic system of the GaAs(110)(1×1) surface, using the cluster shown in figure 6.1b. Dangling bonds were again saturated with hydrogen atoms. Atoms 1Ga and 1As were allowed to move independently in both the (110) and (001) directions. Table 6.2 again shows that the non-self-consistent method produces results in good agreement with existing calculations.

We now repeated the calculations employing the self-consistent ASED method. The results are displayed in table 6.3.

The differences between the non self-consistent and self-consistent cases are negligible. This is important as it suggests that the many iterations involved in the self-consistent formalism, which are costly in terms of computer time, are not necessary and may be replaced by the simple non self-consistent ASED method which makes only light demands on computational resources.

However, the over relaxation of the silicon surface is significant. Trial calculations on the Haber-Bosch process (NH_3 on Fe(111)) and on NH_3 on W(100) have

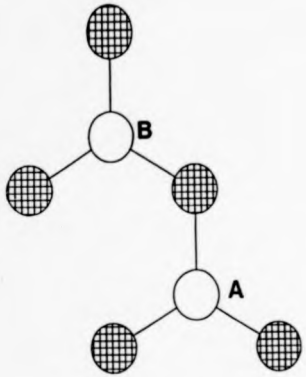

a) Si_7H_{14} Cluster

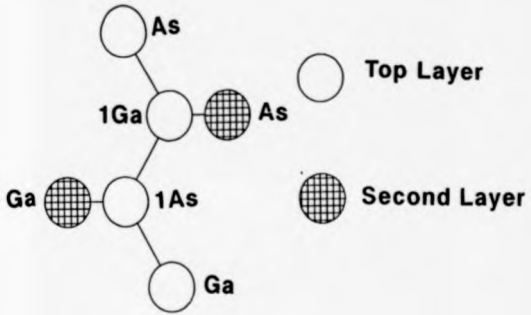

b) $Ga_3As_3H_{12}$ Cluster

Figure 6.1. The Surface Clusters Used to Test the ASED Method

Si(111)(2×1)	A(111)Å	B(111)Å
Non Self-Consistent Tight Binding [16]	+0.24	-0.33
Non Self-Consistent Tight Binding [104]	+0.31	-0.44
Self-Consistent Tight Binding [102]	+0.02	+0.02
Self-Consistent Density Functional [105]	-0.26	-0.26
Non Self-Consistent ASED	-0.44	-0.44

Table 6.1. Comparison for Si(111)(2×1) of calculated atomic displacments. See figure 6.1a for atom labels.

shown that this phenomena is wide spread, and imply that the ad hoc adjustments of the orbital exponents is still necessary to extract realistic bond lengths from the method. Perhaps the main value of the technique lies in its ability to rapidly sort through a large parameter space in the optimisation of complex systems, and suggest a few candidate structures which can then be studied in more detail using the ab initio methods of earlier chapters, rather than producing definitive results by its self.

GaAs(110)(1×1)	1As(110)λ	1As(001)λ	1Ga(110)λ	1Ga(001)λ	Θ
Non Self-Consistent Tight Binding [16]	0.23	0.20	-0.40	0.34	25.9°
Non Self-Consistent Tight Binding [104]	0.19	0.19	-0.46	0.35	27.4°
Self-Consistent Tight Binding [102]	0.19	0.16	-0.32	0.28	21.3°
Ab Initio Hartree Fock [20]	0.22	0.37	-0.44	0.48	26.8°
Non Self-Consistent ASED	0.26	0.20	-0.28	0.37	23.5°

Table 6.2. Comparision for GaAs(110)(1×1) of calculated atomic displacements. See figure 6.1b for atom labels.

Si_7 Cluster	ASED	SCF-ASED
A(111)λ	-0.44	-0.44
B(111)λ	-0.44	-0.44
Ga_3As_3 Cluster		
1Ga(110)λ	0.26	0.25
1Ga(001)λ	0.20	0.21
1As(110)λ	-0.28	-0.26
1As(001)λ	0.37	0.34
Θ	23.5°	21.0°

Table 6.3. Comparison of calculated atomic displacements for the non self-consistent and self-consistent ASED methods.

Chapter 7

Conclusions and Future Work

7.1 Summary

The structure of formate on Cu(100) had been the subject of much controversy with a very unusual cross bridge site being proposed by Outka et al [7] and a more normal bridge site being favoured by Woodruff et al [9]. The use of ab initio Hartree-Fock theory showed conclusively that the Woodruff model was the more stable, and gave a Cu-O bond length of 1.90$\AA$, in agreement with the experimental data.

In the case of methoxy on Cu(100) less was known experimentally, and hence the method was used in a predictive manner. We propose a four fold bridge site with the methoxy group being normal to the surface forming Cu-O bonds of 1.99$\AA$

in length. We also suggest that at room temperatures a non-equilibrium mixed phase may be observed experimentally in which both the two fold bridge and the four fold hollow sites are occupied as had been tentatively suggested by Outka et al [7].

For oxygen on Cu(110) at low temperatures, we propose a dissociative chemisorption process in support of Mundenar et al [13] in which the oxygen atoms sit at the long bridge sites on the surface with a Cu-O bond length of 1.80$\AA$, in contrast to the work of Prabhakaran et al [12] who favoured a molecular adsorbate system.

Finally, for oxygen on Si(100) we propose a new 2×1 structure at low coverage, in which the oxygen atom chemisorbs at the dimer bridge site and sits virtually in the surface plane. The silicon-silicon surface to sub-surface bonds are tilted by about 12.5° with respect to the surface normal. At higher coverages, the dimer and non-dimer bridge sites become equivalent giving rise to the transition from a 2×1 to a 1×1 pattern observed experimentally using LEED. At these higher coverages the oxygen atoms move away from the surface being some 0.725$\AA$ above the surface when all the dimer and non-dimer sites are occupied in agreement with the band structure calculations of Batra et al [80].

A semi-empirical scheme has also been developed which is based on Anderson's ASED method but includes a crude form of charge self-consistency. This has been shown to lead to little improvement in the quality of the results, and hence we

conclude that adjustments of the input ionisation potentials following Pauling's electronegativity theorem is sufficient. However, the problem of the need for large, and unjustified (except on an empirical level), shifts in the input atomic orbital exponents remains. While not negating the value of the method, the need to adjust two different sets of input parameters must cast some doubts over the use of the method in a fully predictive capacity.

7.2 Future Extensions

We are now in a position where the number of possible systems open to investigation is virtually limitless. The ab initio cluster method is ideal for the study of relatively small and simple systems, while the ASED method can be used to generate a few candidate structures for more complex systems, containing many degrees of freedom, which can then be studied in detail with the ab initio techniques.

Perhaps the most interesting area of investigation is the field of additives and poisons in catalytic systems. These are of fundamental importance to the industrial application of catalysis and have recently begun to be investigated experimentally. Very few theoretical studies have been performed, and some interesting questions about how these substances work have still to be answered. (e.g why do small quantities of potassium dramatically increase the productivity of ammonia in the Haber-Bosch process, and why to small amounts of sulphur so effectively

poison carbon-monoxide reactions on nickel surfaces.) These multi-component systems obviously contain many degrees of freedom and hence, the ASED scheme would be used to reduce the parameter space which would then be searched for the correct structure using the full power of the ab initio methods.

On the theoretical front, the obvious development is an efficient scheme for the inclusion of pseudopotentials into ab initio Hartree-Fock theory. Pseudopotentials have formed the basis of virtually all band structure calculations, but have seen little application in the field of quantum chemistry where all electron calculations have been the norm.

Recently, codes including pseudopotentials have become available [33], but problems still appear to exist. In particular, the choice of a basis set is by no means clear cut. It appears that a single diffuse function needs to be added to the standard atomic set in an ad hoc manner ion order to produce realistic results. Hence, more work is necessary before the these methods can be used to produce high quality predictive results.

7.3 Concluding Remarks

This thesis has demonstrated the power of ab initio methods applied to cluster models of chemisorption. The method has been applied both as an aid to interpretation of experimental data (formate on Cu(100) and oxygen on Cu(110)) and as a

predictive tool to obtain information about systems for which little experimental data exists (methoxy on Cu(100) and oxygen on Si(100)).

A self consistent version of the ASED scheme has been developed and it is suggested that the full power of cluster techniques becomes available when the two types of calculation (ab initio and semi-empirical) are used in conjunction for the study of many component systems containing many degrees of freedom.

References

1 G.C. Bond Heterogeneous Catalysis (Oxford University Press, Oxford 1987)

2 D.A. King, D. P. Woodruff (eds) The Chemical Physics Of Solid Surfaces and Heterogeneous Catalysis (Elsevier, Amsterdam 1982)

3 J. H. Sinfelt Prog. Sol. Stat. Chem. 10 (1976) 55

4 H. Froitzheim The Chemical Physics of Solid Surfaces and Heterogeneous Catalysis (Elsevier, New York 1988) eds D. A. King, D. P. Woodruff, p 202

5 M. Bouker, R. J. Madix Surface Sci. 102 (1981) 542

6 J. Stohr, D. Outka, R. J. Madix, U. Dobler Phys. Rev. Lett. 54 (1985) 1256

7 D. A. Outka, R. J. Madix, J. Stohr Surface Sci. 164 (1985) 235

8 M. D. Crapper, C. E. Rilley, D. P. Woodruff Phys. Rev. Lett. 57 (1986) 2598

9 D. P. Woodruff, C. F. McConville, A. L. D. Kilcoyne, Th. Lindner, J. Somers, M. Surman, G. Paolucci, A. M. Bradshaw Surface Sci. 201 (1988) 228

10 A. Wander, B. W. Holland Surface Sci. 199 (1988) L403

11 A. Wander, B. W. Holland Surface Sci. 203 (1988) L637

12 K. Prabhakaran, P. Sen, C. N. R. Rao Surface Sci. 177 (1986) L971

13 J. M. Mundenar, A. P. Baddorf, E. W. Plummer, L. G. Sneddon, R. A. Didio, D. M. Zehner Surface Sci. 188 (1987) 15

14 A. Wander Surface Sci. 216 (1989) L347

15 K. C. Pandey Proc. 17th Int. Conf. Physics of Semiconductors
Eds D. J. Chadi, W. A. Harrison (Springer, New York 1985) p55

16 D. J. Chadi Phys. Rev. Lett. 41 (1978) 1062

17 P. V. Smith, A. Wander Surface Sci. in press

18 L. Pauling Nature of the Chemical Bond (Cornell University Press, Ithaca N.Y.

19 e.g. D. R. Hamann, L. F. Mattheis Phys. Rev. Lett. 54 (1985) 2517

20 C. A. Swarts, T. McGill, W. A. Goddard III Surface Sci. 110 (1981) 400

21 e.g. R. F. Marshall, R. J. Blint, A. B. Kunz Solid Stat. Commun. 8 (1976) 731

22 W. Adams J. Chem. Phys. 34 (1961) 89

23 W. Kohn, L. J. Sham Phys. Rev. 140A (1965) 1133

24 J. W. D. Connolly, J. R. Sabin J. Chem. Phys. 56 (1972) 5529

25 J. B. Danese J. Chem. Phys. 61 (1974) 3071

26 C. C. J. Roothaan Rev. Mod. Phys. 23 (1951) 69

27 J. A. Pople, R. K. Nesbet J. Chem. Phys. 22 (1954) 571

28 S. F. Boys Proc. Roy. Soc. A200 (1950) 542

29 I. Shavitt Methods in Computational Physics eds B. Alder, S. Fernbach,
M. Rotenburg (Academic Press, New York 1963)

30 S. Husinaga J. Chem. Phys. 42 (1965) 1293

31 J. A. Pople Applications of Electronic Structure Theory
eds H. F. Schaefer III (Plenum Press, New York 1977)

32 J. S. Binkley, R. A. Whiteside, R. Krishnan, R. Seeger, H. B. Schlegel, D. J. Defrees, J. A. Pople Gaussian 80 program 406, Quantum Chemistry Program Exchange, Indiana University.

33 M. F. Guest, J. Kendrick Computational Science Group, SERC, Daresbury Laboratory, Warrington, UK.

34 V. R. Saunders, I. H. Hillier Int. J. Quant. Chem. VII (1973) 699

35 P. O. Lowdin Phys. Rev. 97 (1955) 1474

36 W. J. Hehre, L. Salem, M. R. Willcot J. Am. Chem. Soc. 94 (1974) 4328

37 R. J. Bartlett Ann. Rev. Phys. Chem. 32 (1981) 359

38 A. Szabo, N. S. Ostlund Modern Quantum Chemistry (MacMillan, New York 1982)

39 H. Luth, G. W. Rubloff, W. D. Grobman Surface Sci. 63 (1977) 325

40 G. W. Rubloff, J. E. Demuth J. Vac. Sci. Technol. 14 (1977) 419

41 G. B. Fisher, T. E. Madey, B. J. Waclawski, J. T. Yates in Proc 7th Intern. Vac. Congr. Vienna 1977 vol II p1071

42 W. F. Egelhoff, J. W. Linnet, D. L. Perry Faraday Discussions Chem. Soc. 60 (1975) 127

43 G. Blyholder, L. D. Neff J. Phys. Chem. 70 (1966) 893

44 I. E. Wachs, R. J. Madix J. Catalysis 53 (1978) 208

45 I. E. Wachs, R. J. Madix Appl. Surface Sci. 1 (1978) 303

46 R. G. Greenler J. Chem. Phys. 37 (1962) 2094

47 N. Takezawa, H. Kobayashi J. Catalysis 25 (1972) 179

48 H. Ibach, H. Hopster, B. Sexton Appl. Surface Sci. 1 (1977) 1

49 H. Ibach, S. Lehwald J. Vac. Sci. Technol 15 (1978) 407

50 B. A. Sexton Surface Sci. 88 (1979) 299

51 S. Anderson, M. Persson Phys. Rev. B24 (1981) 3659

52 J. Paul, A. Rosen J. Catalysis 84 (1983) 288

53 J. Stohr, J. L. Gland, W. Eberhardt, D. Outka, R. J. Madix, F. Sette, R. J. Koestner, V. Doeber Phys. Rev. Lett. 51 (1983) 2414

54 R. Ryberg Phys. Rev. B31 (1985) 2545

55 A. Madhukar Solid Stat. Commun. 16 (1975) 461

56 K. A. R. Mitchell Surface Sci. 92 (1980) 79 and 100 (1980) 225

57 T. H. Upton J. Chem. Phys. 83 (1985) 5084

58 M. D. Crapper, C. E. Riley, D. P. Woodruff, A. Puschmann, J. Haase Surface Sci. 171 (1986) 1

59 M. D. Crapper, C. E. Riley, D. P. Woodruff Surface Sci. 184 (1987) 121

60 M. D. Crapper, C. E. Riley, D. P. Woodruff J. Phys. C8 (1986) 487

61 A. L. D. Kilcoyne, D. P. Woodruff, Th. Lindner, J. Somers in press Surface Sci.

62 S. Huzinaga Gaussian Basis Sets for Molecular Calculations
(Elsevier, Amsterdam, 1984)

63 G. A. Barclay, C. H. L. Kennard J. Chem. Soc. (1961) 3289

64 K. Prabhakaran, C. N. R. Rao Surface Sci. 198 (1988) L971

65 C. N. R. Rao, P. V. Kamath, S. Yashonath Chem. Phys. Lett. 88 (1982) 13

66 P. V. Kamath, C. N. R. Rao J. Phys. Chem. 88 (1984) 464

67 A. Spitzer, H. Luth Surface Sci. 118 (1982) 121

68 A. Spitzer, H. Luth Surface Sci. 118 (1982) 136

69 C. Backx, C. P. de Groot, P. Biloen Surface Sci. 104 (1981) 300

70 J. L. Gland, B. A. Sexton Surface Sci. 95 (1980) 587

71 J. M. Mundenar, E. W. Plummer, L. G. Sneddon, A. P. Baddorf,
D. M. Zehner, G. R. Gruzalski Surface Sci. 198 (1988) L309

72 J. F. Wendelken Surface Sci. 108 (1981) 605

73 K. C. Prince, G. Paolucci J. Electron Spectrosc. Related Phenom. 37 (1985) 181

74 C. Mariani, H. V. Middelman. M. Iwan, K. Horn Chem. Phys. Lett. 93 (1982) :

75 J. Kanski, L. Ilver, P. O. Nilsson, Solid Stat. Commun. 26 (1978) 339

76 B. A. Sexton J. Vacuum Sci. Technol. 16 (1979) 1033

77 E. G. Keim, L. Wolterbeek, A. van Silfhout Surface Sci. 180 (1987) 565

78 V. Barone, F. Lelj, N. Russo, M. Toscano Surface Sci. 162 (1985) 230

79 N. Russo, M. Toscano, V. Barone, F. Lelj Phys. Lett. 113A (1985) 321

80 I. P. Batra, P. S. Bagus, K. Hermann Phys. Rev. Lett. 52 (1984) 384

81 K. Ibach, H. D. Bruchmann, H. Wagner Appl. Phys. A29 (1982) 113

82 C. M. Garner, I. Lindau, J. N. Miller, P. Pianetta, W. E. Spicer
J. Vacuum Sci. Technol. 14 (1977) 372

83 C. M. Garner, I. Lindau, C. Y. Su, P. Pianetta, W. E. Spicer
Phys. Rev. Lett. 40 (1978) 403

84 C. Y. Su, P. R. Skeath, I. Lindau, W. E. Spicer
J. Vacuum Sci. Technol. 18 (1981) 843

85 T. Kunjunny, D. K. Ferry Phys. Rev. B24 (1981) 4604

86 J. A. Schaefer, F. Stucki, D. J. Frankel, W. Gopel, G. J. Lapeyre
J. Vacuum Sci. Technol. B2 (1984) 359

87 J. A. Schaefer, W. Gopel Surface Sci. 155 (1985) 535

88 M. Chen, I. P. Batra, C. R. Brundle J. Vacuum Sci. Technol. 16 (1979) 1216

89 T. Kunjunny, D. K. Ferry Phys. Rev. B24 (1981) 4593

90 S. Ellialtioglu, S. Ciraci Solid Stat. Commun. 42 (1982) 879

91 S. Ciraci, S. Ellialtioglu, S. Erkoc Phys. Rev. B26 (1982) 5716

92 A. S. Bhandia, J. A. Schwarz Surface Sci. 108 (1981) 587

93 V. Barone Surface Sci. 189 / 190 (1987) 106

94 B. I. Craig, P. V. Smith Surface Sci. in press

95 R. M. Tromp, R. J. Hamers, J. E. Demuth Phys. Rev. Lett. 55 (1985) 1303

96 R. J. Hamers, R. M. Tromp, J. E. Demuth Phys. Rev. B34 (1986) 5343

97 M. J. Frisch, J. A. Pople, J. S. Binkley J. Chem. Phys. 80 (1984) 3265

98 R. Hoffman J. Chem. Phys. 39 (1963) 1397

99 A. B. Anderson J. Chem. Phys. 62 (1975) 1187

100 A. B. Anderson, R. W. Grimes, S. Y. Hong J. Phys. Chem. 91 (1987) 4245

101 W. A. Harrison Phys. Rev. B31 (1985) 2121

102 V. M. Dwyer, J. N. Carter, B. W. Holland Proc. 2nd Inter. Conf. Struc. Semiconductor Surfaces eds J. F. Van der Veen, M. A. Van Hove Springer Series in Surface Sci. 11 (1988) 320

103 D. G. Anderson J. Assoc. Comput. Mach. 12 (1964) 547

104 J. N. Carter, V. M. Dwyer, B. W. Holland Surface Sci. 188 (1987) L723

105 K. C. Pandey Phys. Rev. Lett. 49 (1982) 223

TITLE Cluster Studies of Chemisorption Using Total Energy Techniques

AUTHOR Adrian Wander

INSTITUTION and DATE University of Warwick 1989